

## Design and Fabrication of an Adaptive Leading Edge Rotor Blade

Sridhar Kota, Gregory Ervin, Russell Osborn  
FlexSys Inc., Ann Arbor, Michigan, 48105  
[kota@flxsys.com](mailto:kota@flxsys.com)

Robert A. Ormiston  
Aeroflightdynamics Directorate (AMRDEC)  
U.S. Army Research Development and Engineering Command  
Ames Research Center, Moffett Field, CA 94035  
[ormiston@mail.arc.nasa.gov](mailto:ormiston@mail.arc.nasa.gov)

### Abstract

Using Compliant Systems, a variable geometry leading edge was developed for a high performance Sikorsky SSC-A09 rotor blade that morphs to an aerodynamically optimized 10-degree cambered profile (for ideal performance in the blade-retreated position) once per revolution. The variable geometry allows the blade to maintain an optimal profile throughout its entire azimuthal circuit, delaying blade stall and thereby offering substantial gains in forward speed, maneuverability, and payload capacity.

### Background and Technical Approach

Compliant systems are single-piece, flexible structures (or joint-less mechanisms) with discrete or embedded actuation schemes that are designed to generate desired motions upon application of external forces. A compliant system includes one or more compliant transmissions or mechanisms integrated (or embedded) with actuators, with or without control schemes.

Compliant mechanisms, if properly designed and manufactured, are well suited for highly repeatable and accurate motion applications like wing leading and trailing-edge surfaces, as well as other aircraft components, such as inlets, where variable geometry is required. Their unitized construction without joints makes their manufacture simple, eliminating most of the complex assembly operations. Additionally, the compliant surface provides a smooth aerodynamic contour, free of steps and discontinuities associated with traditional joints [1, 2].

A mathematical framework and a systematic, semi-automated approach to designing compliant structures for Continuous Shape Generation (CSG) problems was

developed. CSG problems involve *synthesis* of a suitable structure in order to produce a required shape change – while minimizing actuation forces, and maximizing coupling stiffness between aerodynamic loads and actuators. In addition, material and stability constraints must also be satisfied. The approach is based on structural optimization techniques in which the compliant structure problem is broken into topology synthesis and size and geometry synthesis to arrive at a final detailed structural design [3, 4].

The majority of research in adaptive structures has not exploited the elasticity of the underlying structures. FlexSys developed a variable geometry trailing edge for a fixed wing aircraft using compliant structures. The design, called Mission Adaptive Compliant Wing (MACW) was successfully flight tested in December 2006 [5]. In contrast to conventional elastic mechanisms that employ flexible hinges, the Mission Adaptive Compliant Wing (MACW) uses sophisticated algorithms to design the topology and shape of an internal structure that deforms as a whole rather than concentrating the flexion in localized regions, avoiding high-stress concentrations. The MACW technology provides lightweight, low power, variable geometry re-shaping of the upper and lower flap surface with no seams or discontinuities. The wing was tested at full-scale dynamic pressure, full scale Mach, and reduced-scale Reynolds Numbers on the Scaled Composites White Knight aircraft. Testing revealed laminar flow was achieved over approximately 60% of the airfoil chord for much of the lift range. Analysis and test results suggest significant fuel savings, weight savings and a higher control authority [5]. The same underlying technology is now being applied to design and development of variable geometry leading edge for a rotorcraft.

Numerical studies using the OVERFLOW 1.8ab code have shown that an adaptive, drooping rotor leading edge design holds significant aerodynamic promise. Results obtained for the SSC-A09 airfoil show that, with proper leading edge droop control provided by a compliant leading edge system, the airfoil can achieve a higher

---

\*Presented at the American Helicopter Society 64<sup>th</sup> Annual Forum, Montreal, Canada, April 29 – May 1, 2008. Copyright © 2008 by FlexSys, Inc. All rights reserved.

maximum lift coefficient than the baseline airfoil section. In addition, the morphing technology can eliminate the dynamic stall vortex and result in a lift coefficient equivalent to the base section's maximum lift coefficient [6].

Figure 1 illustrates the aerodynamic benefit of a morphing rotor blade [7]. By taking into consideration the full scale air loads and 1000g centrifugal load, a compliant structure was designed for 220 million morphing cycles and a 3-ft span bench-top model was fabricated with +/- 10 degree deflection capability running at 6Hz. The D-spar was moved rearward 8.5% to make room for the compliant structure and actuator hardware. The total peak power consumed by the flap is estimated to be 885 Watts for a 7-foot span flap, which weighs 13.8 lb and is driven by a 34 lb linear electromagnetic actuator located at the base of the rotor.

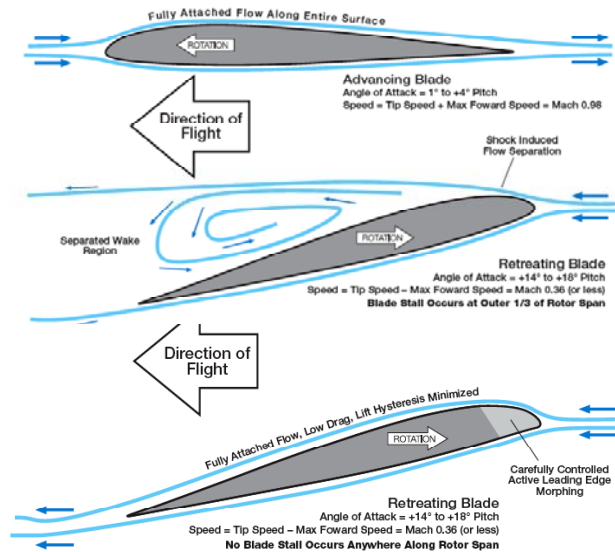


Figure 1: Cambering the leading edge as the blade retreats delays dynamic stall and keeps the flow attached.

### Design Considerations

Designing an adaptive control surface for a rotorcraft poses many challenges due to limited space, weight constraints, and centrifugal loads. The primary objective is to design an efficient structure, which can distribute local actuation power to the surface of the airfoil to produce a specified shape change. The system must provide appropriate shape control over the adaptive surface while meeting power, weight, packaging, and survivability constraints. Based on aerodynamic analysis and optimization, the ideal shapes of the airfoil are first established. A full-scale model of SSC-A09 rotor blade (including the pressure loading, centrifugal forces etc) was used in establishing the design requirements and in designing the compliant structure and actuator. The

design process takes into account the performance requirements and the constraints listed below:

I. Shape morphing: (a) D-Spar location, (b) Required shapes for stall elimination, (c) Wear strip location (top or bottom, % chord), (d) Compliant structure topology/geometry to effect shape change.

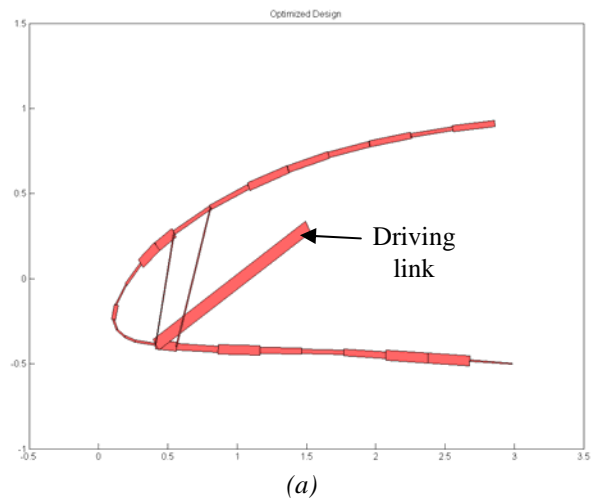
II. Power required to achieve deflection: (a) Pressure loading, (b) Required deflection (10 degrees, 5 degrees), (c) Response time (5 Hz to 7 Hz), (d) Required compliant structure stiffness (aeroelastic & dynamic constraints).

III. Packaging issues: (a) Available actuator power density (ultrasonic rotary, electromagnetic, inchworm, etc.), (b) D-Spar location, and (c) Actuator system architecture.

IV. Durability and dynamic performance: (a) Structural integrity of LE flap, (b) Dynamic/Aeroelastic response & fatigue loading.

### Topology Design

Using proprietary topology synthesis methods, a preliminary topology was generated starting with desired shapes. Figure 2 shows the driving link and the beam elements connecting upper and lower surfaces of the leading edge. Figure 2(b) shows the cambered shape as the driving link is rotated counter-clockwise. The topology and actuation system are protected under US patent 5,971,328 with other US and foreign patents pending [8].



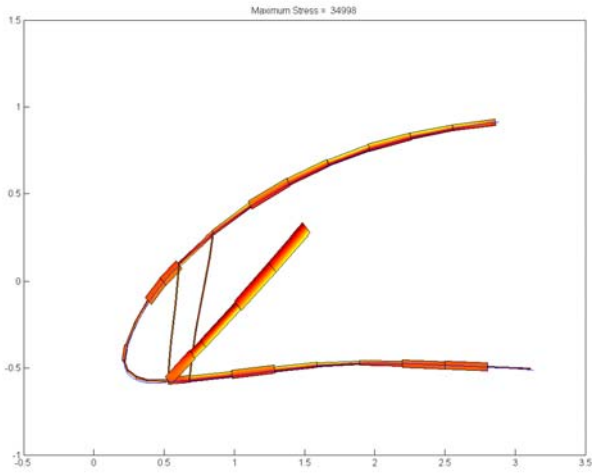


Figure 2: (a) Optimized topology; (b) 10 degree cambered position as the driving link is rotated.

Structural analysis of the optimized topology was carried out using ANSYS analysis software. Model loads included the appropriate maximum pressure loads at the 0 and 10 degree position and a 1000 G spanwise acceleration load. Figure 3 illustrates the von Mises stress distribution of the beam model with the combined loading. Stresses in the zero degree position indicate the need for further size and shape optimization to reduce stresses.

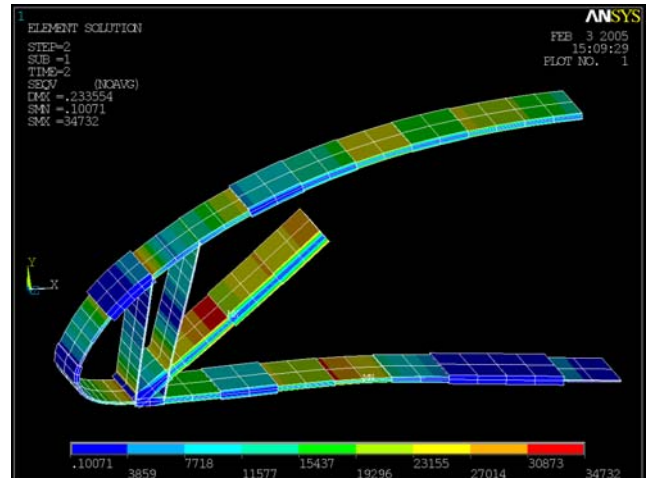
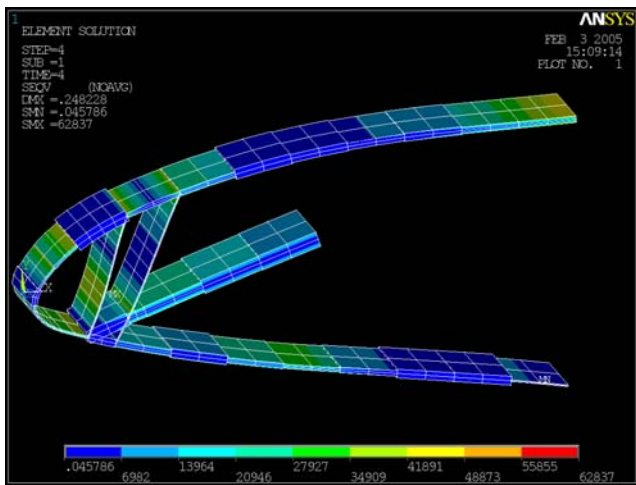


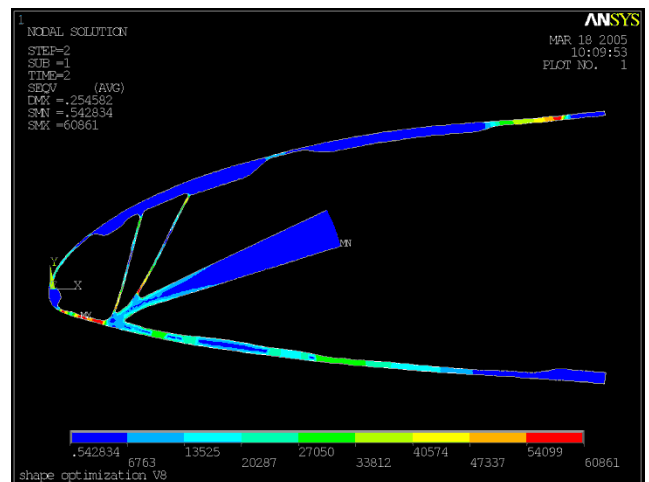
Figure 3: ANSYS 3D nonlinear beam model with 1000 G acceleration-(a) 0 degree flap; (b) 10 degree flap.

### Shape Optimization

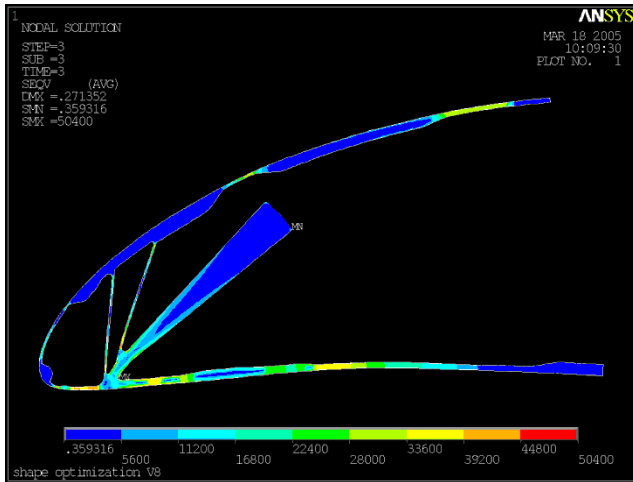
A final detailed shape optimization was performed to (a) reduce stresses and (b) to improve shape matching of the ten degree deformed shape – which was shown to improve the time-dependent (cyclic) lift and pitching moment performance of the airfoil. The final shape optimization altered the maximum stress values to 60.9 ksi (420 MPa) at 0 degrees position and 50.4 ksi (347 MPa) at 10 degree positions. At a 7 Hz operating speed, the instantaneous peak power draw was calculated at 684 Watts for a 2 meter span flap (aerodynamic and structural loads only). At 5 Hz, this power draw reduces to 488 Watts. Figure 4 illustrates the von Mises stress distribution model within the continuum model at the 0 and 10 degree position.



(a)



(a)

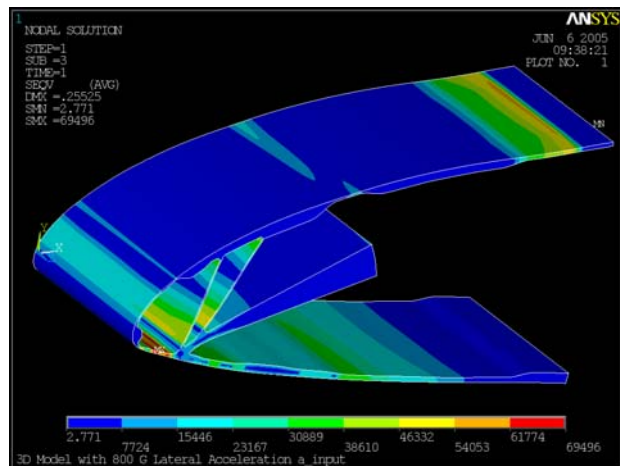


(b)

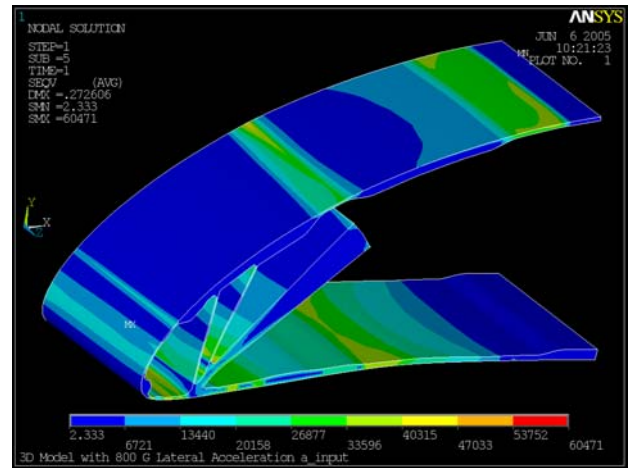
Figure 4: Secondary shape optimized results – von Mises stress plot-(a) 0 degree flap; (b) 10 degree flap (US patent 5,971,328 and other US and foreign patents pending).

### Three-Dimensional Simulation

Detailed (continuum) three-dimensional simulation of the leading edge structure was re-examined to assess the stresses / strains in an individual compliant rib due to pressure loading and centrifugal loading. An equivalent stress plot is shown in Figure 5 of the model in the 0 degree and 10 degree flap position, with maximum pressure load and an 800 G lateral acceleration applied to the model. The structural simulation predicts a maximum equivalent stress of 69.5 ksi (479 MPa) compared to 60.9 ksi (420 MPa) for the 2D continuum analysis with no lateral acceleration. This maximum stress produces a static factor of safety of 1.84 compared to the yield strength of the Ti 6-4 material, 128 ksi (880 MPa). This factor of safety increases to 2.50 for static loading.



(a)



(b)

Figure 5: Von Mises stress distribution of 1 inch wide 3D compliant structure in 0 degree position and 10 degree position (US patent 5,971,328 and other US and foreign patents pending).

Alternative titanium alloys were investigated to increase static and fatigue strength. After conducting a thorough search of titanium alloys, a Ti-10V-2Fe-3Al alloy was selected due to its superior static and fatigue strength. This alloy has a yield strength of 174 ksi (1200 MPa) and a 145 ksi (1000 MPa) 1E6 cycle fatigue strength which extrapolates to a 75 ksi (517 MPa) fatigue strength at 220 million cycles.

Figure 6 illustrates the stress life fatigue data from the 3D finite element model following the stresses at each node in the model from the 0 degree flap position to the 10 degree flap position. For the Ti-6V-4Al material a handful of points in the model are in violation of the required cyclic life. However, the Ti-10V-2Fe-3Al material is within the 220 million (SF=2) fatigue strength line.

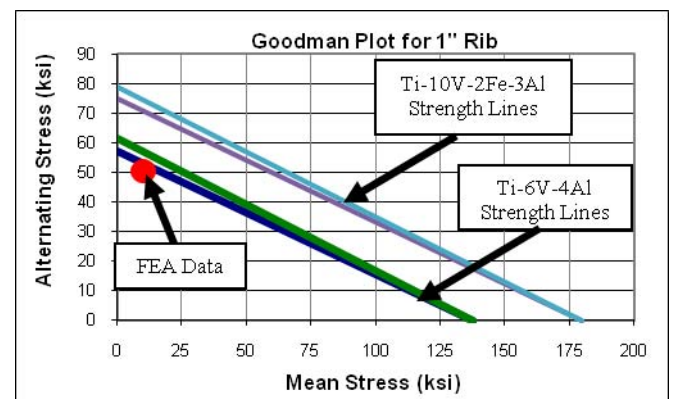


Figure 6: Stress life plot for mean and alternating stress for detailed 3D compliant rib model.

Further stress studies were conducted with differing rib width (and differing acceleration loading). Two-dimensional plane strain analyses were compared to three-dimensional analysis – with the three-dimensional analyses still carrying approximately a 7.5% increase in stress. Further studies of stress convergence using different three-dimensional element type and meshes were limited due to the computational time needed for solving nonlinear structural models. The overall assumption is that the three-dimensional stress results are slightly elevated and should represent a conservative estimate of the stress levels present in the rib.

### CAD Design of Full-Scale Compliant Leading Edge Flap System

#### CAD Model

Given the tight space constraints, high power requirements, and limitations associated with selecting off-the-shelf bearings, shafting, etc. the leading edge spar was moved backward an additional 0.097 inches pushing the D-spar back to 9.0%. To meet these design requirements, an actuation system was designed that converts a linear span wise motion in to a rotary motion for actuation of the flap. A linear slide contacts bearings in a cam-wedge arrangement. The roller bearings ride in an angled groove in the linear rail and when motion is applied, the result is a rotary motion. Figure 7 illustrates the linear rail, and cam-wedge arrangement, viewing the system looking down on top of the airfoil.

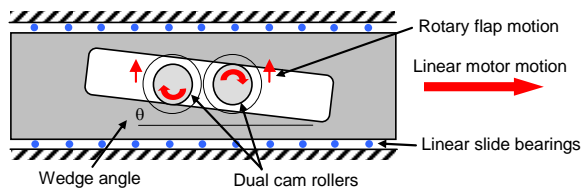


Figure 7: Illustration of actuation system that translates linear motion to rotary motion of the flap.

Bearings were selected to support the cam-wedge loads while operating (rolling) for the 220E6 cycles. Bending, shear, and contact stresses for the cam-roller system are estimated using strength of materials and Hertzian stress calculation approaches. The maximum contact stress is 301,511 psi (~2 GPa) for the cams at the 10 degree flap position under maximum pressure loading. There are a few specialty carburized and hardened steels that can meet these very high contact stress values. A CAD model of the preliminary component selection model is shown in Figure 8.

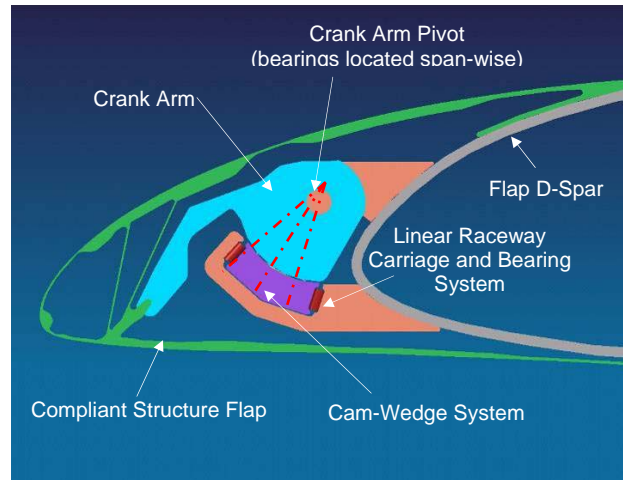
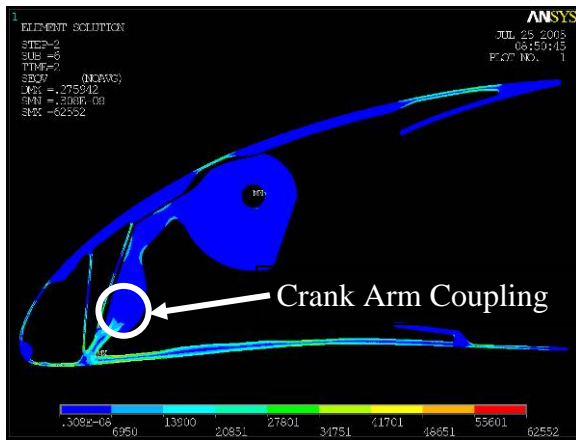
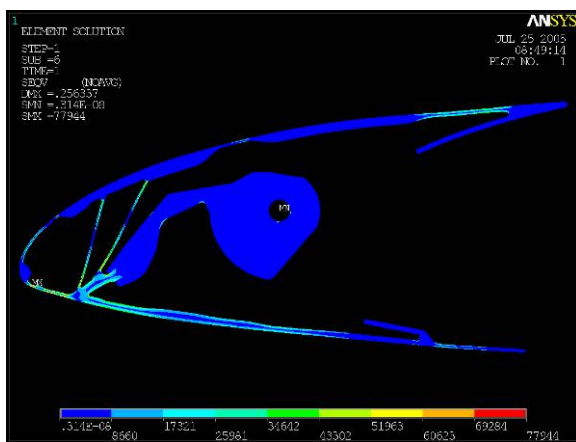


Figure 8: CAD model of leading edge flap cam wedge system and D-spar.

Finite element modeling of the leading edge flap and the CAD modified crank arm (for packaging considerations to avoid interference) was undertaken in order to examine stresses in the flap due to separation of the crank arm through a tear-dropped shaped coupling. Figure 9 illustrates a finite element model of the crank arm and compliant flap as well as the detail of the coupling between the two components. A 0.004” gap between the arm and the mechanism will be bonded using a high strength adhesive. Finite element analysis modeled this adhesive layer to examine shear stress in the bond layer (maximum of 3000 psi which can be adequately handled using a high strength adhesive like Hysol or another aerospace grade adhesive). Using a mesh refined 6-node triangular plane stress element, the maximum von Mises stress levels in the mechanism were predicted to be 78 ksi – which are 31% higher than the structurally optimized flap with the integrated flap and crank arm (this stress increase only appears in the 0 degree position). Clearly, further structural optimization could be performed in order to reduce this peak stress level. However, the stress levels are adequate for the bench-top demonstration prototype (will not fail for > 1 million cycles).



(a)



(b)

Figure 9: (a) Finite element model of the crank arm coupled to the compliant structure via an adhesive layer (+10 degrees deflection); (b) Finite element model of the crank arm-compliant structure (0 degrees deflection).

### Actuator Selection and Concept Integration

In order to provide a suitable actuation system that fits within the tight packaging constraints and meets the durability and power density requirements, a thorough study was conducted of different actuator technologies including, electromagnetic actuators -rotary and linear systems, piezoelectric, and electrostrictive materials coupled with compliant motion amplification technology to achieve the necessary force-displacement characteristics. Additionally, exploiting dynamic resonance effects to minimize actuator peak power requirements was investigated (this assumes a periodic response from the leading edge system).

A promising method to actuate the leading edge flap is to provide longitudinal motion along the rotor blade span using a push rod in constant tension. This method allows an actuator to be located inboard away from high centrifugal force locations. While investigating various actuation strategies, the motion of the actuator (linear,

rotary, or other) along with the system packaging must be considered in order to develop an appropriate method for coupling the motion of the actuator together with the compliant structure. The actuator characteristics were then fed into the compliant mechanism design algorithms to optimize the system performance.

Linear electromagnetic actuators, voice coil actuators and piezoelectric actuators all generate linear output motion with varying magnitudes of output forces and displacements. The final actuator choice was based on many factors including: reliability/durability, force/displacement required to drive the compliant LE, need for a transmission system, packaging, weight (including drive electronics) and power capability. Different solutions may exist due to the specific consideration (criterion) and trade-offs. Comparisons were made among these solutions and the final choice was a linear electromagnetic actuator. In addition, research has been conducted concerning the use of electromechanical actuators for deforming leading edge structures in rotor blades [9]. Much was learned from this research about electromechanical actuators in rotorcraft applications.

Given the actuator force and power requirements, a linear electromagnetic motor from Anorad (Rockwell Automation) LC-50-300 was selected. The dimensions and weight of this actuator are: 2.12" x 3.15" x 15" and would weigh 15.5 lb (9.8 lbm is included in the dynamic analysis as the stator mass). Inboard mounting of the actuator would require a local bulge in the airfoil to accommodate the added volume forward of the D-spar.

### Final Design

A variable camber compliant structure leading edge flap for dynamic stall alleviation was successfully designed and fabricated. This flap modifies the baseline SSC-A09 rotor blade airfoil to provide 0 to 10 degrees of flap motion for an 8.5% chord flap. The flap can be actuated at rates up to (and exceeding) 6 Hz to provide once per rev flap positioning. At the 10-degree position, the shape of the flap allows the airfoil to generate additional lift at higher angles of attack than the baseline (no flap) airfoil. The total peak power consumed by the flap (under aerodynamic loading and 6 Hz actuation rate) is estimated to be 885 Watts for a 7-foot span flap. The total weight of the 7-foot flap design is 33.8 lbs. of which the compliant structure and the transmission weighs about 13.8 lbs. and the linear electromagnetic actuator is approximately 20 lbs with the majority of the system mass located at the base of the rotor – away from high centrifugal loads. Future (recommended) testing includes static and dynamic wind tunnel testing to validate the retreating blade lift enhancement as well as fatigue and whirl stand

testing (Mach scaled and full scale) to mature this technology.

### Bench-top Prototype

The primary goal of the bench-top model is to demonstrate the performance of the leading edge flap in a durable and easily transportable package. The prototype has a 3 foot span, 18 inch chord model (full-scale) with a 1 foot span adaptive leading edge flap as shown in Figure 10. The model is powered to drive the flap from 0 Hz to 6 Hz flap rate. The flap morphs at a fixed cycle from 0 degrees to 10 degrees deflection. Due to time and budget constraints, the bench-top prototype differs from the “real” flap in the following manner:

- A rotary actuator (Maxon EC 32) was used to provide cyclic flap actuation.
- The D-spar was machined from aluminum rather than fabricated from composites.
- The coupling between the crank arm and the compliant structure has been simplified to a rectangular geometry (simplifies machining).
- The linear race way incorporates PTFE polymer bearings. Ideally a re-circulating roller bearing system would be developed

The rest of the prototype model adheres closely to the full-scale rotorcraft-caliber system.

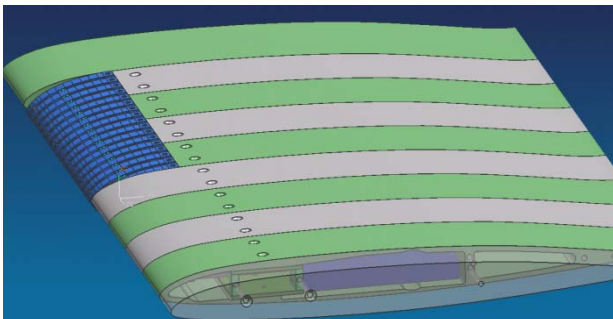


Figure 10: Bench-top prototype.

Twenty five titanium ribs were machined through wire EDM machining. These ribs were inspected for machining accuracy using a micrometer. Measurement error for thin webs is on the order of 0.0002” to 0.0004” indicating excellent tolerance capability. The bench top prototype employed a Maxon DC motor, a linkage and a cam-wedge transmission system that was successfully tested up to the top speed of the motor – which correlates to a 6 Hz reciprocating frequency.

The cam-wedge rail required precision 5-axis machining with heat treatment to increase hardness and super finishing on Teflon bearing surfaces. Figure 11 shows the D-spar and crank arm (with bearings). The cam-wedge

and linear raceway are shown lying on top of the D-spar. In the background of the picture is the rotary to linear actuation system.

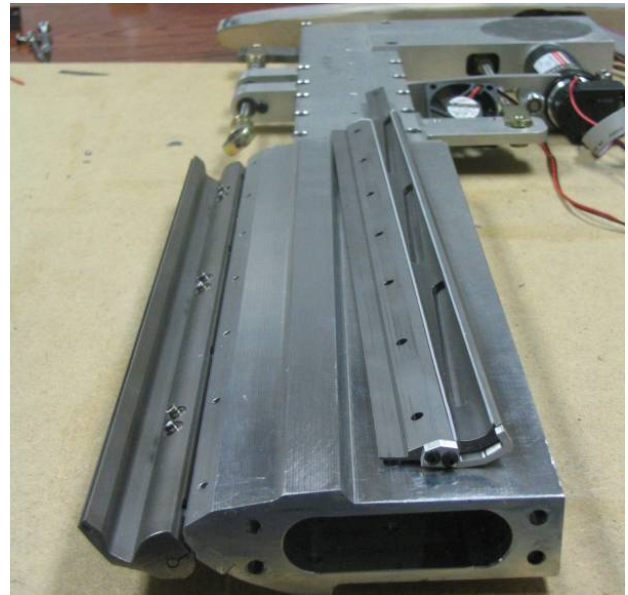


Figure 11: The D-spar, crank-arm and cam-wedge linear transmission system

The next several processes involved assembling the cam-wedge and bonding the titanium ribs to the D-spar. Finally a 0.005” polycarbonate skin was bonded to the model using an epoxy adhesive combined with vacuum bagging equipment. The final assembled bench-top model is shown below in Figure 12.



(a)



(b)

Figure 12: Bench-top model showing- (a) 0 degree and; (b) 10 degree flap positions.

### Bench-top Prototype Measurement

Before the bench-top model was covered with the polycarbonate skin, the model was mounted on a manual Brown and Sharpe Coordinate Measuring Machine (CMM) to measure the 0, 5, and 10 degree flap positions. The model was squared to the CMM base and the flap was measured by taking roughly 30 to 40 points along the surface. The accuracy of the CMM is rated at  $\pm 0.00016$  inch. Figure 13 shows the raw points measured from the flap at the 5 degree position. Note that the coordinate frame was different from the finite element models and the data was transformed accordingly.

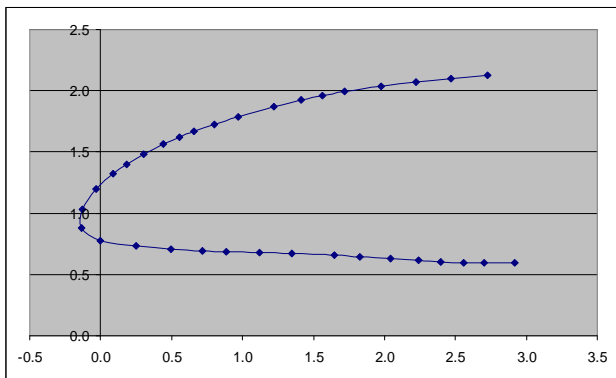


Figure 13: Raw CMM point Data

Figures 14 and 15 show a comparison of the measured flap surface to the predicted finite element models for the 0 degree and 10 degree flap position. Note that the curves are not an exact match. The primary reason for the shift is due to backlash in the cam-wedge system and it can be eliminated by increasing the travel of the wedge to design in “over stroke” capability.

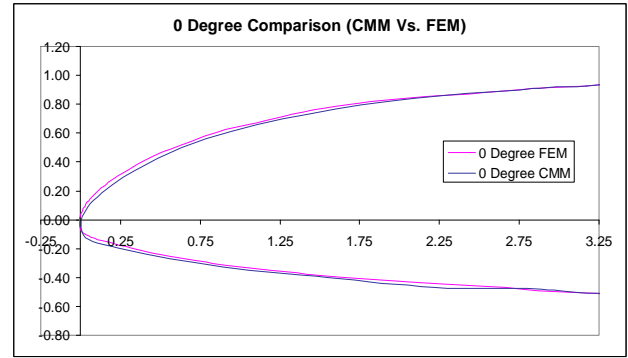


Figure 14: Comparison of CMM and FEA leading edge profiles at 0 degrees.

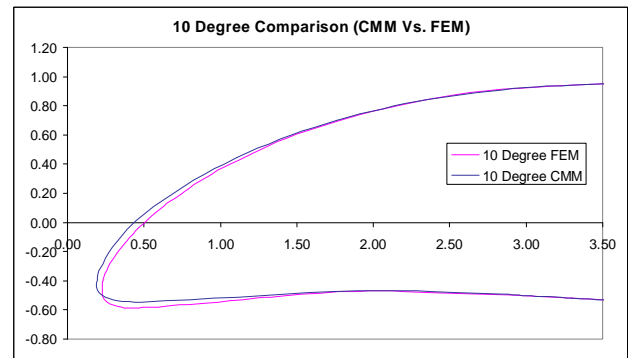


Figure 15: Comparison of CMM and FEA leading edge profiles at +10 degrees.

### Conclusions and Recommendations

The variable geometry leading edge designed by FlexSys based on aero optimized target shapes provided by Rolling Hills Corporation, provides up to a 35 percent increase in retreating blade lift with no stall and no negative hysteresis in lift, pitching moment, or drag. This technology has the capability to increase the combination of top speed, maximum payload, and altitude capability of all rotorcraft. Further study of this work is needed to assess the level of performance increase given targeted (benchmark) vehicles. We demonstrated the feasibility of compliant systems technology by successfully designing and fabricating a prototype bench-top model which demonstrates the 6 Hz flap rate.

Rotorcraft are extremely complex, dynamic vehicles that require sophisticated analysis, design, testing, and re-testing when implementing new technologies. Additional aerodynamic (static & dynamic) and structural testing (fatigue, Mach-scaled whirl stand and full scale whirl stand) as well as future design iterations will be needed to mature this adaptive structure flap technology to a level where it can be implemented on a full scale rotorcraft.

### Acknowledgements

This work was carried out as a US Army SBIR Phase II sub contract to FlexSys Inc. The authors are appreciative of the aerodynamic analysis and airfoil optimization work performed by Rolling Hills Research Corporation, CA. The authors gratefully acknowledge the technical guidance of Dr. Preston Martin, Aeroflightdynamics Directorate (AMRDEC), U.S. Army Research Development and Engineering Command.

### References

1. Kota, S., Hetrick, J., Osborn, R., "Adaptive Structures: Moving into Mainstream, Aerospace America, September 2006, pp16-18.
2. Kota, S., Hetrick, J., Osborn, R., Paul, D., Pendleton, E., Flick, P. and Tilmann, C., "Design and Application of Compliant Mechanisms for Morphing Aircraft Structures," Paper 5054-03, *SPIE Smart Structures and Materials Conference on Industrial and Commercial Applications of Smart Structures Technologies*, San Diego CA, 2-6 March 2003.
3. Hetrick J., and Kota S., "An Energy Efficiency Formulation for Parametric Size and Shape Optimization of Compliant Mechanisms", ASME Transactions, *Journal of Mechanical Design*, June 1999, Vol.21, pp.229-234.
4. Hetrick, J., Kota, S., "Topological and Geometric Synthesis of Compliant Mechanisms," *ASME Design Engineering Technical Conference*, MECH-14140, Baltimore, Maryland, Sept. 10-13, 2000.
5. Hetrick J., R.F. Osborn, S. Kota, P. Flick, D. Paul, "Flight Testing of Mission Adaptive Compliant Wing, 48th AIAA/ASME/AHS/ASC Structures, Structural Dynamics, and Materials Conference, Honolulu, Hawaii, April 2007.
6. Kerho, M., "Adaptive Airfoil Dynamic Stall Control," AIAA 2005-1365, presented at 43rd AIAA Aerospace Sciences Meeting, January 10-13, 2005, Reno, NV.
7. Reuster, J., Baeder, J., "Leading Edge Deformation for Dynamic Stall Control," AIAA Paper 2001-0120, *39th Aerospace Sciences Meeting and Exhibit*, Reno, NV, January 8-11, 2001.
8. Kota, S., "System for Varying a Surface Contour," U.S. Patent No. 5,971,328, Oct 26, 1999.
9. Fink, David A.; Reinhardt, Nicholas; Severance, Randy; Phillips, Robert; Gaudreau, Marcel P.J.; and Ormiston, Robert A.; "Deformable Leading Edge Electromechanical Airfoil," paper presented at the American Helicopter Society 63rd Annual Forum, Virginia Beach Virginia, May 1-3 2007.